First-principles study of the dependence of silicon electronic transport properties on the crystallographic growth

Núria García Castelló
Dr. Albert Cirera Hernández, Departament d'Electrònica, Universitat de Barcelona
Dr. Joan Daniel Prades García, Departament d'Electrònica, Universitat de Barcleona

Abstract— **Differences in the electronic transport properties of two polymorphs of bulk silicon due to the crystallographic direction are investigated theoretically. The calculations are performed in two steps: first an optimized geometry for two polymorphs of silicon (cubic diamond and hexagonal diamond) is obtained using DFT calculations, and then the transport relations of four directions (<001>, <110> and <111> for diamond and <001> for hexagonal) are obtained using NEGF approach. SIESTA and TranSIESTA simulation codes are used in the calculations correspondingly. The electrodes are chosen to be the same as the central region where transport is studied, eliminating current quantization effects due to contacts and focusing the electronic transport study to the intrinsic structure of the material. By varying chemical potential in the electrode regions, an I-V curve is traced for each particular configuration. Conductance in silicon bulk shows certain dependence in the crystallographic direction, in agreement with the different behavior of silicon nanowires due to their growth direction. The study of electronic and transport properties in silicon nanowires is interesting because they are promising candidates as bridging pieces in nanoelectronics.**

Index Terms—**1. Modeling and simulation of systems and properties of matter at the nanoscale: DFT, conductance, electronic transport, growth direction, I-V characteristic, NEGF, polymorphs, silicon.**

I. INTRODUCTION

The current interest in Silicon Nanowires (SiNWs) is mainly derived from their technological potential in nanoscale devices [1]-[4]. Bottom-up nanowires growth techniques allows overcoming the limit of conventional lithography-based top-down design [5] leading to a leap forward in terms of miniaturization [6].

SiNWs belong to a unique class of semiconductor nanowires because they are integrable within the conventional silicon-based device technologies. In fact, the experimental realization of SiNW electronic devices has been achieved recently [7], [8]. For this reason, SiNWs represent a particularly attractive class of building blocks for nanoelectronic devices, such as field-effect transistors (FETs) [4], [7]- [9], passive diode structures [9], integrated logical circuits [10] and biosensors [11], [12].

To date, SiNWs have been synthesized in a wide range of diameters and crystallographic growth directions: <100> [13], [14], <110> [13]-[16], <111> [15]-[17] and <112> [15], [16]. It has been observed that nanowire growth direction shows diameter dependence [18]. Nanowires with diameters less than about 20 nm show preferential growth in <110> direction [19], whereas thicker SiNWs with diameters larger than about 50 nm tend to grow along the <111> direction [15].

Concerning the crystal structure, high resolution transmission electron microscopy experiments revealed that most of the SiNWs have single-crystalline bulk structures [14], [15]. In contrast with the intuition, depending on the size and growth conditions, the crystalline structure could differ from the diamond-like cubic, which is the typical in bulk Si. Recently, *ab-initio* studies predicted that diamond-structure nanowires are unstable for diameters smaller than 1nm [20]. There also exist experimental evidences that SiNWs can grow in a hexagonal diamond type structure [21]: Arbiol *et al*. [22] for Cu-catalyzed Vapour-Solid-Solid (VSS) grown SiNWs and Fontcuberta i Morral *et al.* [23] for Au-catalyzed Vapour-Liquid-Solid (VLS) grown SiNWs.

Therefore, on the one hand, it is possible to integrate SiNWs in novel nanoelectronic devices. On the other hand, current synthesis techniques can furbish us with a wide range of SiNWs with radically different crystallographic and electronic properties. However, very little is known about the impact of these structural properties on the behavior and performance of the final device [5], [24].

Recently, the first studies dealing with this timely question have been published. Justo *et al.* [25] reported classical molecular dynamics simulations of the stability of SiNWs with various surface facet families and orientations. Sorokin *et al.* [26] computed the electronic band structure of different facets of SiNWs with density functional theory calculations. Svinhenko *et al.* [27] studied the conductivity of small diameter (0,46-1,56 nm) SiNWs in <110>, <111> and <100> directions using Non-Equilibrium Green's Function techniques within tight-binding approximation, demonstrating that the differences in the band structure of each direction strongly affects the current-voltage characteristics of ideal NWs.

However, technical limitations in the integration of ultra-thin SiNWs (diameter < 15 nm) in real devices hinders the applicability of these results [28].

Here, we present a theoretical study of the electron transport properties of bulk Si along the most significant growth directions of SiNWs, in order to cover the gap between the minute dimensions of current atomistic models of nanowires (diameter < 4 nm) and the typical sizes of real nanodevices (diameter > 15 nm). In the latter range, the electric transport phenomena are still dominated by the bulk properties, being bulk-Si a good approximation to mimic the transport properties in thick SiNWs [29]. Therefore, here the electronic transport is studied inside an open-boundary bulk system described by first-principles field within Non-Equilibrium Green's Functions (NEGF) formalism [30]. For the shake of completeness, the most significant growth directions and polymorphs of SiNWs, namely cubic diamond phase oriented along $<001>_d$, $<110>_d$ and $<111>_d$ axis and hexagonal diamond phase along $<001>_h$ have been considered. The differences in the I-V curves obtained with each configuration and their technologic consequences are discussed in detail.

II. Calculation Details

Our first-principles calculations were performed in the framework of Density Functional Theory [31], [32] (DFT) as implemented in the SIESTA (Spanish Initiative for Electronic Simulations with Thousands of Atoms) code [33], [34]. It implements the standard Kohn-Sham self-consistent method in the Generalized Gradient Approximation (GGA) for the exchange-correlation functional [35] in the PBEsol (Perdew-Burke-Ernzerhof for solids) parametrization [36], and norm-conserving Troullier-Martins pseudopotentials [37] in their fully non-local Kleinman-Bylander factorization form [38] to represent the electron-ion interaction. Solutions of the Kohn-Sham's equations were expanded as Linear Combinations of Atomic Orbitals (LCAO) of finite range, with a kinetic energy cutoff of 0,02 Ry [39]. Silicon atoms were described by 4 valence electrons plus the corresponding pseudo-potential ion charges. The basis set used was double ζ plus polarization, which is the most common basis in this kind of calculations [20].

Table I shows the simulation parameters used for each configuration.

TABLE I
Simulation Parameters

Parameters	Cubic diamond (227, Fd $\bar{3}$ m)			Hexagonal diamond (186, $P6_3mc$)
Direction	<001>	<110>	<111>	<001>
Mesh Cutoff (Ry)	200	200	200	150
Kgrid cutoff (Ang)	10	10	10	20
Monkhorst-Pack set (electrode)	4x4x4	6x6x4	6x6x3	11x11x7
Monkhorst-Pack set (system)	4x4x1	6x6x1	6x6x1	11x11x1

In SIESTA, k-point sampling is controlled by the k-grid cut-off parameter defined as half the length of the smallest lattice vector of the supercell required to obtain the same sampling precision with a single k-point [40]. This k-grid cut-off generates the corresponding Monkhorst-Pack set [41]. Real space mesh cut-off [33], [34] and k-grid values were set to converge total energy values within 0,1 meV and maximum absolute forces over atoms (calculated as analytical derivatives of the total energy [42]) better than 0,004 eV/Ang in all cases.

The electronic transport properties were studied with Non-Equilibrium Green's Function (NEGF) techniques, within the Keldysh formalism [43], based on DFT as implemented in the TranSIESTA package [44]. It computes the electronic transport properties of a nanoscale system confined in a central scattering region (C) in contact with two semi-infinite left (L) and right (R) electrode regions at different electrochemical potentials. The bias voltage V_b between them corresponds to the electrochemical potential difference between the left (μ_L) and the right (μ_R) electrodes, $eV_b = \mu_L - \mu_R$. In our case, both electrodes (red atoms in Fig. 1) and the contact region (yellow atoms in Fig. 1) were made of Si.

The method is based on the construction of the NEGF using the DFT Hamiltonian and the overlap matrices obtained from a given electron density. Subsequently, a new electronic density is computed using the NEGF formalism, instead of the usual diagonalization procedure, which closes the DFT-NEGF self consistent cycle.

The DFT Hamiltonian can be expressed in the following form

$$\begin{pmatrix} H_L+\Sigma_L & V_L & 0 \\ V_L^{+} & H_C & V_R \\ 0 & V_R^{+} & H_R+\Sigma_R \end{pmatrix} \qquad (1)$$

which contains three different contributions. The two of the electrodes (Hamiltonian matrices $H_{L,R}$ and self energies $\Sigma_{L,R}$, which contain the interaction of the electrode atoms described explicitly in the calculation and the remaining part of the semi-infinite electrodes) are determined from a previous bulk calculation with periodic boundary conditions. The one corresponding to the interaction between electrode-contact region $V_{L,R}$ and the Hamiltonian of the contact region H_C are both computed explicitly with TranSIESTA Green Functions in an open boundary system.

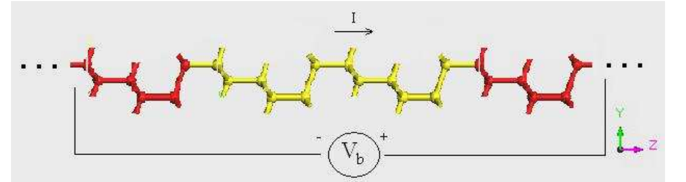

Fig. 1. Configuration of the transport model for the cubic diamond <111> direction, 24 atoms in total: 1 unit cell/electrode (red) and 2 unit cell in the contact region (yellow). The electrochemical potential difference between the left and right electrodes is linked to an external bias voltage V_b.

TABLE II
DESCRIPTION OF THE STRUCTURES

<001>$_d$	8 atoms/unit cell	2 unit cell/electrode	2 unit cell in contact region	6 unit cell in total (48 atoms)
<110>$_d$	4 atoms/unit cell	3 unit cell/electrode	3 unit cell in contact region	9 unit cell in total (36 atoms)
<111>$_d$	6 atoms/unit cell	1 unit cell/electrode	2 unit cell in contact region	4 unit cell in total (24 atoms)
<001>$_h$	4 atoms/unit cell	2 unit cell/electrode	2 unit cell in contact region	6 unit cell in total (24 atoms)

The current I through the contact region was calculated using the Landauer-Buttiker formula [45],

$$I(V_b) = G_0 \int_{\mu_R}^{\mu_L} T(E, V_b) dE \qquad (2)$$

where $G_0 = 2e^2/h$ is the unit of quantum conductance, and $T(E,V_b)$ is the transmission probability of electrons incident at an energy E through the device under the potential bias V_b. Finally, the transmission function is obtained with a post-processed tool, TBTrans [39], which uses the self-energies of the electrodes and the green functions of the whole system.

III. METHODOLOGY

First, exhaustive tests were carried out to determine the minimum simulation parameters (see Table I) required to describe properly the two silicon polymorphs. Cubic diamond (International Table number 227, space group Fd$\overline{3}$m) with initial experimental lattice parameter [46] of a = 5,4309 Å was relaxed with SIESTA (by conjugate gradient minimization of the energy until maximum absolute forces over atoms were better than 0,004 eV/Ang in all cases) to a = 5,48156 Å. Hexagonal diamond (IT number 186, space group P6_3mc) with initial experimental lattice parameter [23] of a = 3,8 Å and c=6,269 Å was optimized to a = 3,854497 Å and c=6,367122Å. Cell angles did not display any significant variation after relaxation.

As regards to the thermodynamic stability of each polymorph, the total energy per atom of the hexagonal diamond structure was 0,01 eV/atom greater than the corresponding value for the cubic diamond phase, in total agreement with previous GGA calculations [20] and with the fact that hexagonal diamond is a metastable phase of Si [16].

These lattice parameters were used to build the atomistic models needed in the TranSIESTA calculation. Two important criteria were taken into account to design each model [39]:

1. The electrodes must be large enough to guarantee that orbitals within the unit cell only interact with one single nearest neighbor cell.
2. The scatter region has to be large enough to avoid the interaction between left and right electrode.

The main features of the four structures generated using these criteria are summarized in Table II: cubic diamond <001>$_d$, <110>$_d$ and <111>$_d$ directions, and hexagonal diamond <001>$_h$ direction. Subindices d and h are used to refer to each phase throughout this work. It is noteworthy, that the assumption of these widely accepted criteria leads to the constructions of unit cells containing different numbers of atoms, both in the electrodes and in the central region, for each different direction. As discussed below, precautions have been taken to minimize the influence of these effects on the here-reported results. Fig. 1 shows the structure of the whole transport model for the <111>$_d$ direction (left and right electrodes and contact region). The cross section of each direction is represented in Fig. 2 (in all cases, the transport direction is along z axis).

After building the structural models, a self consistent field of the electrodes in periodic boundary conditions was calculated to obtain the density matrix, the real-space Hamiltonian (H_L and H_R) and the self-energies (Σ_L and Σ_R). These data were used in subsequent calculations to compute the surface Green's functions of the electrodes.

Afterwards, the process was repeated for the whole system (left and right electrode and contact region) to obtain the non-equilibrium electron density matrix (in open boundary conditions) of the system and the remaining parts of the Hamiltonian (H_C, V_L and V_R).

Finally, the electron transmission function and the current flowing along the previous structure in constant bias conditions (V_b) were calculated with the help of the post-processing tool TBTrans, included in the TranSIESTA package. As suggested by some authors [47], [48], the I-V characteristic of the material (current values at different bias conditions) was obtained iterating the previous process for different V_b values. We increased V_b in steps of 0,1 V and used the converged density matrix of the previous state as an initial guess for the next step [47], [39].

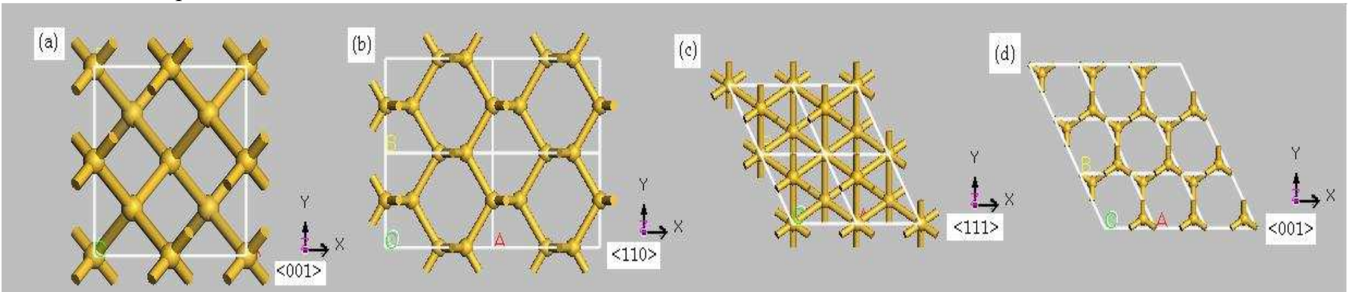

Fig. 2. *Cross section of each configuration. (a) cubic diamond in <001> direction, 8 atoms/unit cell; (b) cubic diamond in <110> direction, 4 atoms/unit cell; (c) cubic diamond in <111> direction, 6 atoms/unit cell; (d) hexagonal diamond in <001> direction, 4 atoms/unit cell. In all cases, the electronic transport is along the z axis.*

IV. Results and Discussion

A. Interpretation of the results obtained with TranSIESTA

The theoretical framework that lays behind the TranSIESTA code includes a number of approximations and assumptions that must be taken into account to make meaningful interpretations of the results. In this section, we describe the most widely accepted way of interpreting the electron transport properties predicted with TranSIESTA. For simplicity we will focus in the results obtained for <110>$_d$, the rest of the results can be consistently interpreted in the same way.

In the conductance function (Fig. 3) we can see that there's a zero-transmission region of 0,8 eV (± 0,4 eV around the Fermi level) that directly corresponds with the computed band gap ($E_{gap\ <110>d}$ = 0,793 eV, as known, underestimated by DFT). In the current-voltage curve that value is the voltage at which the intensity increases significantly (Fig. 4). However, we can see that there are non-zero values of the current from 0,5 V. That is in agreement with the conductance function, where there is a little but significant non-zero transmission above these energies (Fig. 3).

This behavior is clearer if we compare the conductance at different bias voltages (Fig. 5). The conduction and valence region of the spectrum are more separated as the bias voltage V_b increases. This occurs because the polarization produces a relative displacement of the electrodes energy bands: the Fermi level of the left electrode is shifted up to $eV_b/2$ and the Fermi level of the right electrode is shifted down to $- eV_b/2$. Hence, the energetic distance between the conduction band of the left electrode and the valence band of the right electrode increases with the bias voltage.

But, at the same time, the energetic distance between the valence band of the left electrode and the conduction band of the right electrode decreases with bias voltage. When there is an overlapping between the valence and conduction states of both electrodes (i.e., when V_b is approximately the band gap), a transmission channel through the contact region is created and there is electron transport from left to right electrode. In these conditions, current starts to flow. In Fig 6 (c) we can see that there is no region of zero-transmission around the Fermi level when the bias voltage is 0,8 V. For greater bias voltage, Fig. 6 (d), there is a region around the Fermi level with transmission, due to the states created by the overlapping of the left electrode-valence band and right electrode-conduction band.

As said before, we can verify that the transmission at 0,5V of bias voltage, Fig. 6 (b), has a little but significant region inside the current integration range with non-zero values of conductance, as long as the energetic distance between the left valence band and the right conduction band has decreased and there are energetic states near the Fermi level that were not available when there was no bias voltage. This region contributes to compute a total current different of zero.

This ON-OFF effect predicted by the simulations is closely related with the fact that DFT is a ground state theory. In this

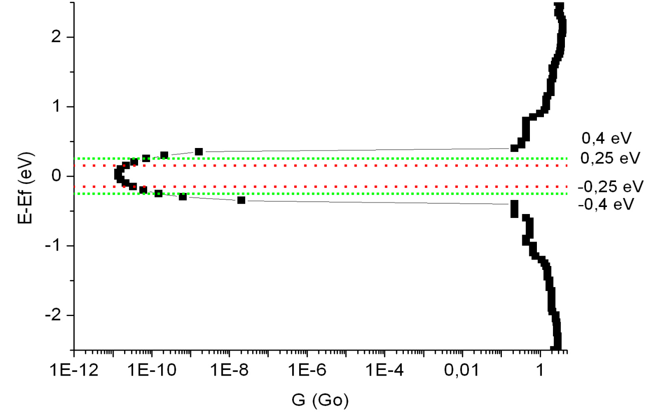

Fig. 3. Conductance along the direction <110> of the cubic diamond at zero bias voltage. The zero-transmission zone (between -0,4 eV and 0,4 eV) is similar to the computed band gap, 0,79 eV. But, at 0,25 and -0,25 eV there's a little but significant electron transmission.

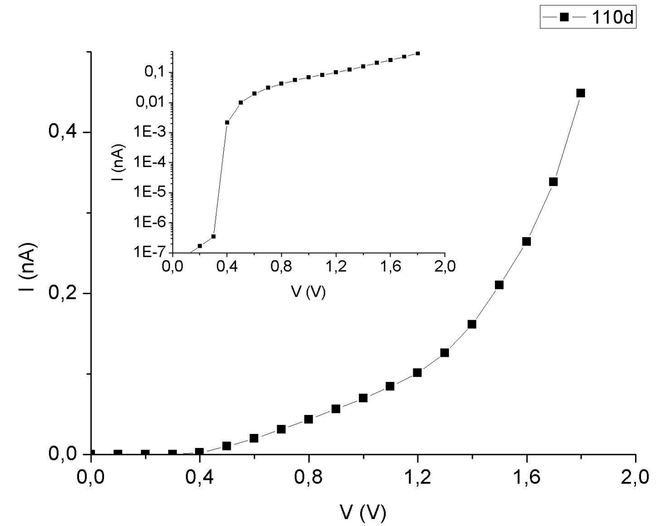

Fig. 4. I-V characteristic of the direction <110> of the cubic diamond. Current starts to have a non-zero value at 0,5V, but it starts to grow up near the energy gap value, 0,8V. Detail of the I-V curve in a logarithmic scale.

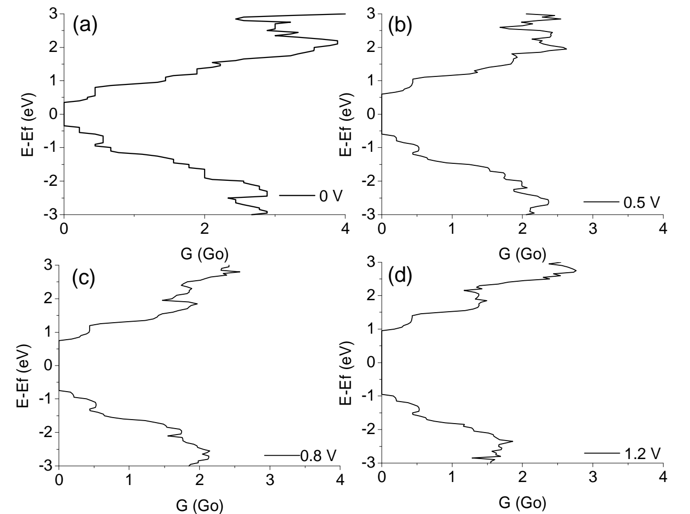

Fig. 5. Conductance of the direction <110> of the cubic diamond at (a) 0V, (b) 0,5 V, (c) 0,8 V and (d) 1,2V of bias voltage. The zero-transmission zone increases with the bias voltage.

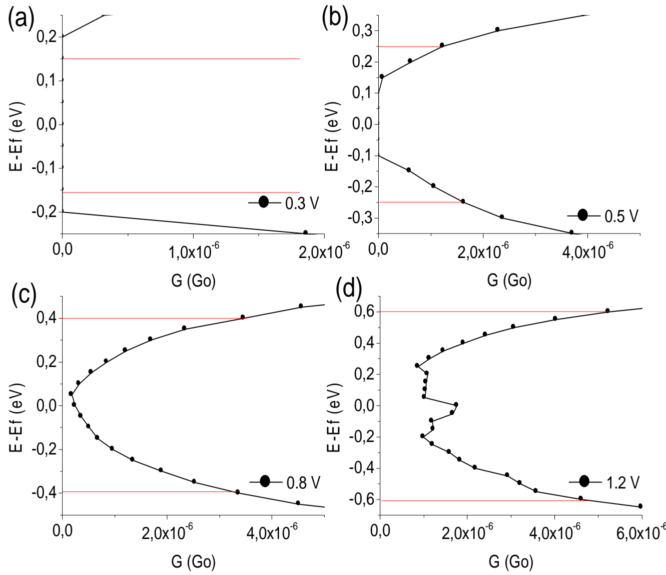

Fig.6. *Detail of the conductance of the direction <110> of the cubic diamond near the region where the integration of the current is done (the red lines correspond to -V_b/2 and V_b/2) at (a) 0,3 V, (b) 0,5 V, (c) 0,8 V and (d) 1,2V of bias voltage.*

such state, the conduction band is strictly empty and the valence band is completely occupied by electrons. This is a crucial difference with the transport in a real material, which always will have a temperature different of 0 K.

B. Comparison of the conductance and I-V characteristic between the different configuration

Our systems have periodic boundary conditions in the plane perpendicular to the transport direction (z axis). TranSIESTA code compute the current in one system cell in the transversal direction, otherwise, the current would be infinite (i.e., the x-y plane is infinite due to the periodic boundary conditions). Thus, to have a finite and comparable magnitude, current values are reported (Fig. 7) in terms of the current per unit cell area transversal (x-y plane) to each transport direction (z axis). The comparison of both the conductance and the I-V curves leads to the same results: the direction $<001>_d$ displays highest conductance and the largest current values at high bias voltages, followed by the direction $<110>_d$, $<001>_h$ and the last one being $<111>_d$.

In the case of the hexagonal polymorph, the $<001>_h$ direction has a narrower zone of zero-transmission, which agrees with the smaller energy band gap computed for this configuration ($E_{gap\ <001>h}$ = 0,34 eV) compared to the diamond-like directions, and with the fact the experimental evidence that this polymorph of silicon has a lower band gap [23].

If we compare the directions of cubic diamond in the region where the bias voltage is lower than the energy gap, the direction $<111>_d$ presents significant current at lower V_b values.

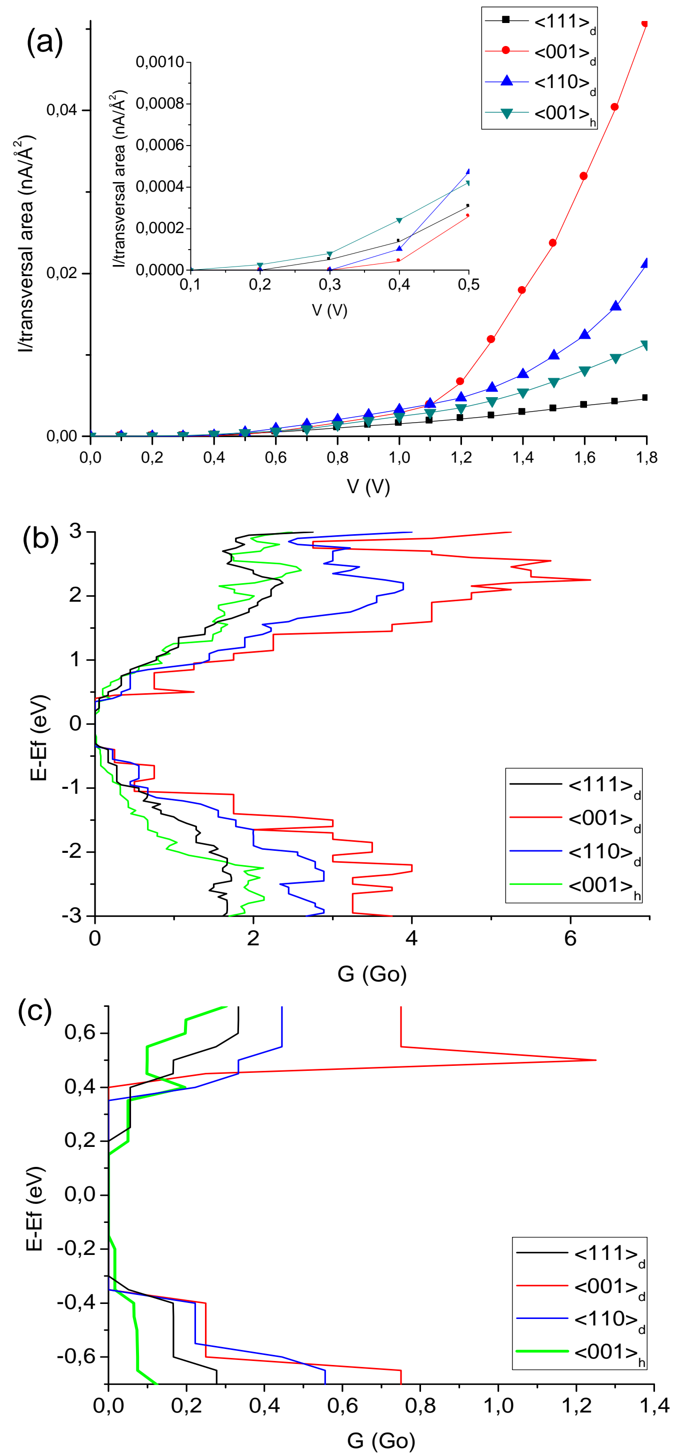

Fig. 7. *(a) Comparison of the I-V characteristic (I in this case is the current per unit of transversal area) of the three directions of cubic diamond $<001>_d$, $<110>_d$ and $<111>_d$ and the hexagonal diamond $<001>_h$. Detail of the I-V curve for low bias-voltage, before current starts to flow significantly. (b) Comparison of the conductance of $<001>_d$, $<110>_d$ and $<111>_d$ and $<001>_h$.(c) Detail of the conductance in the region near the Fermi level. The band gap of hexagonal diamond silicon is lower than the cubic diamond*

C. Influence of the electrodes and contact region size

In order to clarify if the differences in the size of the models constructed for each direction have any significant effect on

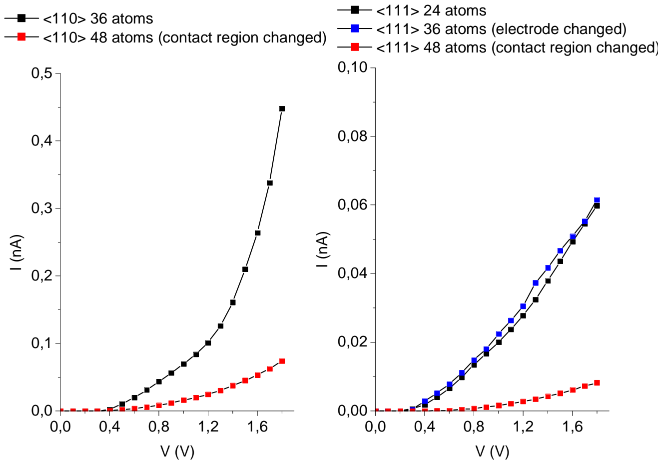

Fig. 8. *Influence of the electrode and contact region size to the current.*

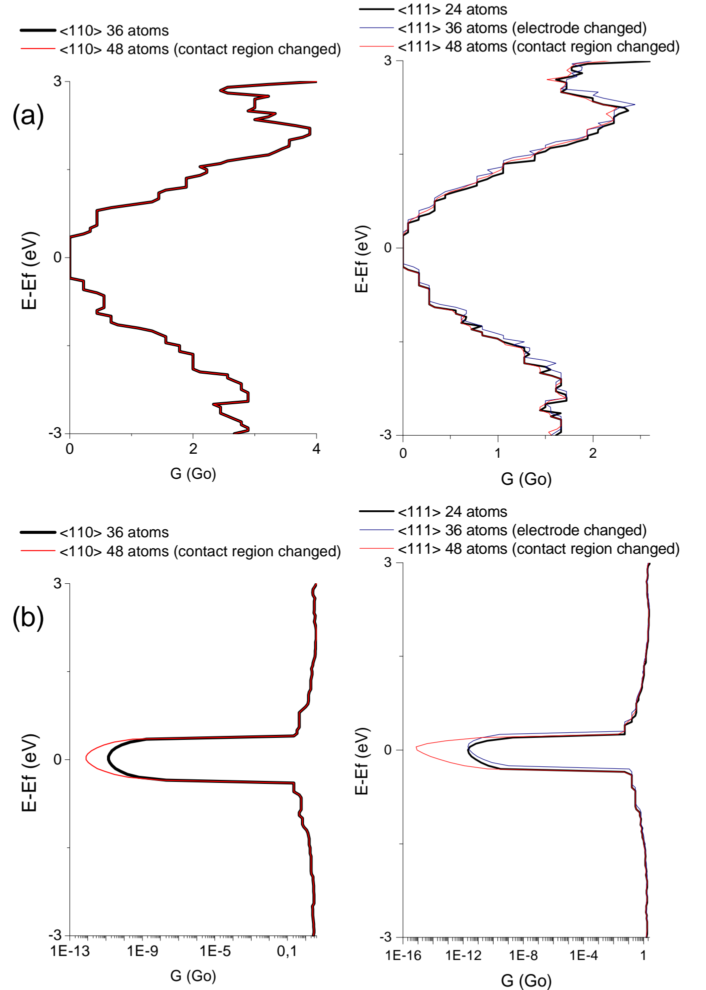

Fig. 9. *(a) Conductance for the direction <111>$_d$ and <110>$_d$ for the original system and the new configurations, where the electrode and the contact region are changed. (b) Logarithmic plot of the dependence with the number of atoms. There's a significant difference in the non-conduction region between the changed-contact region system, and the original and changed-electrode system.*

the transport differences described in the previous section, specific calculations were run.

To study the effect of the number of atoms, we computed two new configurations. The first one had the same contact region than the original but different electrode sizes (<111>$_d$ with twice the electrode: 12 atoms/electrode, 36 atoms in total). In the second one the electrodes remained unaltered and the size of the contact region was increased (<111>$_d$ with three times the contact region: 36 atoms in it, 48 atoms in total; and <110>$_d$ with twice the contact region: 24 atoms in it, 48 atoms in total). We found that changes in the electrode do not produce a significant variation in the current, but an increase of the contact region leads to a decrease in the current (see Fig. 8).

From the point of view of the conductance, Fig. 9 (a), the modified systems display the same general features that the original ones. But, if we center our attention, Fig. 9 (b), in the region where the integration of the current will take place (around the non-conduction region), the system with the modified contact regions seems to be less conductive, in accordance with the results shown in Fig. 8.

Therefore, we conclude that the electrode size does not change the electronic transport. This confirm that our electrodes' models are good enough to study the differences in the electronic transport of the contact region: these electrodes act as a real infinite reservoirs of electrons that can be sent from one side and absorbed in the other, being dispersed by the central region. Thus, upon conduction, electron transport is only limited by the properties of the central scattering region.

In contrast, we have observed that there is a notable diminution of the current with the number of atoms in the contact region. This is a common phenomena, which has already been observed by other authors [27], and might be related to the increase in the scattering centers. It is noteworthy that this effect modifies the quantitative values obtained in the simulation but do not alter at all the qualitative order of the different growth directions, as far as their conductance is concerned.

Finally, as regards the intrinsic variations in the number of atoms of the contact region due to the differences in the crystal structure of each direction (see Table II), it must be beard in mind that each one of these models represents the minimum structural unit in which transport along a given crystallographic direction can be defined. In other words, the relative differences and ordering of the I-V characteristics predicted per structural unit in each direction should still be valid for nanowires with different orientations containing similar number of such elementary transport units. All these guarantee the significance of the results reported in this study.

D. Discussion of the results

We have verified that our methodology is correct to study the electronic transport of our structures. The electrodes behave like a reservoir of electrons and the atoms in the contact region act as elastic scattering centers. In this way, the electronic transport from the valence states of the left electrode

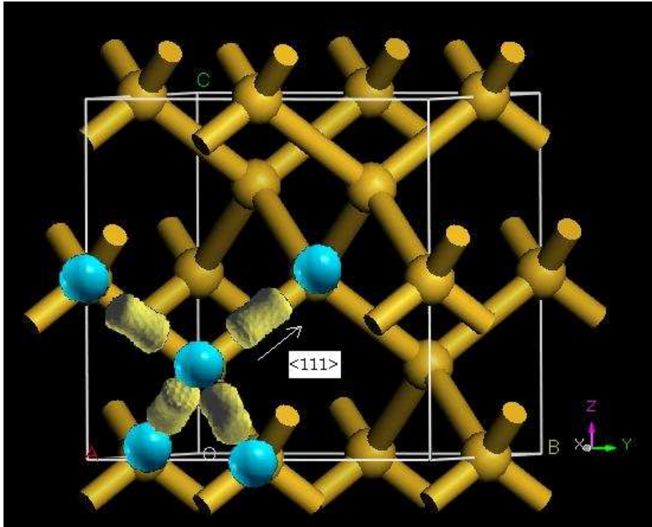

Fig. 10. *Location of the electron charge density (light yellow) in cubic diamond silicon*

to the conductance band of the right electrode along the scatter center region gives us the conductance function of the system. This is the information that we wanted, because, with electrodes of the same material than the central region, it ensures that all transport modes existing in structures are coupled to the device. This type of configuration makes evident the effects over the electronic transport due to the different orientation and order of the atomic orbitals in each crystallographic direction and for the different polymorphs of silicon.

There are several reasons that hamper a quantitative comparison of the results of our calculations with experiments. First of all, the transport model considered does not take into account inelastic scattering effects (which play a key role in the experimental values of the conductance). Second, the DFT assumes 0 K in the calculations, situation that will never be achieved in experiments. Third, as discussed before, there exists a certain dependence of the particular current value predicted by the simulation on the size of the model of the contact region.

Anyhow, as all the models considered in this work were constructed consistently to represent an elementary transport unit in each direction with the same criteria, we can affirm that our results are qualitatively correct. This assertion is supported by other authors in works that discuss about which are the most suitable configurations for modeling and in which similar procedures are reported [44], [47]-[49].

It is not surprising that the first direction that shows significant current values at lower V_b values is the $<111>_d$. This effect can be related with the fact that the electron charge density is concentrated mainly along this direction in cubic diamond-like structures, which have a tetrahedral configuration, see Fig. 10.

From the point of view of the electron conductance, we have observed that the transport direction and structural phase play an important role. First, the $<001>_d$ is the direction that gives more current when conduction is fully activated (bias voltage above the band gap), followed by $<110>_d$, and, quite far away, there are the $<111>_d$ and $<001>_h$.

The most common growth direction reported for SiNWs thinner than 20 nm is $<110>_d$ [19] whereas for SiNWs with diameters greater than 50 nm is $<111>_d$ [15]. Also, SiNWs grown along $<001>_d$ [13], [14] and $<001>_h$ [22], [23] direction can be efficiently synthesized with VLS technique. Therefore, current synthesis methods can furbish experimentalist with nanowires grown in different directions that are expected to display differential transport properties, according to the here-reported results. However, an exhaustive work providing experimental evidences of such effects is still missing in the literature.

V. CONCLUSION

We have studied the electronic transport properties of Si with the help of *ab initio* calculations, within the framework of DFT and NEGF formalism, with the aim of examining the effect of the crystallographic growth direction on the electronic transport.

The conductance function and I-V characteristic of the most significant SiNW growth directions, corresponding to two different polymorphs of silicon (cubic diamond and hexagonal diamond phase) have been studied.

The largest current values for high bias voltages were predicted for the direction $<001>_d$. For the low bias regime, the hexagonal diamond polymorph is the first one to display conduction due to its lower band gap value, followed by the $<111>_d$ direction.

The effects of the number of atoms in the atomistic models on the electronic conduction have been explored in order to check the validity of the here-assumed simulation criteria. We have demonstrated that the electrodes effectively acted as infinite reservoirs of electrons, since the electronic transport properties do not change significantly with their size. In contrast, the current values depend on the size of the scatter central region.

This fact, together with the absence of inelastic scattering effects and the assumption of 0 K intrinsic to theoretical framework make our simulations not quantitatively comparable with experiments, but the results are completely valid from a qualitatively point of view.

To sum up, we have shown how *ab initio* modeling of electron transport can provide theoretical hints and guidelines to improve and taylor the performance of SiNW-based devices, in which the approximation of bulk transport is still valid.

ACKNOWLEDGMENT

The author is grateful to Prof. P. Ordejón and Dr. R. Rurali (ICMAB-CSIC, Spain) for their help in the first steps of the *ab initio* electronic transport calculations and the support of the APIF program of the University of Barcelona.

REFERENCES

[1] S.-W. Chung, J.-Y. Yu, and J.R. Heath, "Silicon nanowire devices", *Appl. Phys. Lett.*, vol. 76, pp. 2068-2070, April 2000.

[2] C.M. Lieber, "Nanowire Superlattices", *Nano Lett.*, vol. 2, pp. 81-82, Feb. 2002.

[3] D. Appell, "Nanotechnology: Wired for success", *Nature*, vol. 419, pp. 553-555, Oct. 2002.

[4] G. Zheng, W. Lu, W, S. Jin, and C.M. Lieber, "Synthesis and Fabrication of High-Performance n-Type Silicon Nanowire Transistors", *Adv. Mater.*, vol. 16, pp. 1890-1893, Nov. 2004.

[5] R. Rurali, "Colloquium: Structural, electronic, and transport properties of silicon nanowires", *Rev. Mod. Phys.*, vol. 82, No. 1, January-March 2010.

[6] C.M. Lieber, "Nanoscale Science and Technology: Building a Big Future from small things", *MRS Bulletin*, pp. 486-491, July 2003.

[7] Y. Cui, S. Hong, D. Wang, W.U. Wang, and C.M. Lieber, "High Performance Silicon Nanowire Field Effect Transistors", *Nano Lett.,* vol. 3, pp. 149-152, Nov. 2003.

[8] T.Y. Liow, *et al.*, "5 nm Gate Length Nanowire-FETs and Planar UTB-FETs with Pure Germanium Source/Drain Stressors and Laser-Free Melt Enhanced Dopant (MeltED) Diffusion and Activation Technique", *Symposium on VLSI Technology Digest of Technical Papers*, pp. 36-37, 2008

[9] Y. Cui, and C.M. Lieber, "Functional Nanoscale Electronic Devices Assembled Using Silicon Nanowire Building Blocks", *Science*, vol. 291, pp. 851-853, Feb. 2001.

[10] Y. Huang, *et al.*, "Logic Gates and Computation from Assembled Nanowire Building Blocks", *Science*, vol. 294, pp. 1313-1317, Nov. 2001.

[11] J. Hahm, and C.M. Lieber, "Direct Ultrasensitive Electrical Detection of DNA and DNA Sequence Variations Using Nanowire Nanosensors", *Nano Lett.*, vol. 4, pp. 51-54, Jan. 2004.

[12] Y. Cui, Q. Wei, H. Park, and C.M. Lieber, "Nanowire Nanosensors for Highly Sensitive and Selective Detection of Biological and Chemical Species", *Science*, vol. 293, pp. 1289-1292, Aug. 2001.

[13] J.D. Holmes, K.P. Johnson, R.C. Doty, and B.A. Korgel, "Control of Thickness and Orientation of Solution-Grown Silicon Nanowires", *Science*, vol. 299, pp. 1471-1473, Feb. 2000.

[14] D.D.D. Ma, C.S. Lee, F.C.K. Au, S.Y. Tong, and S.T. Lee, "Small-Diameter Silicon Nanowire Surfaces", *Science*, vol. 299, pp. 1874-1877, March 2003.

[15] Y. Wu, *et al*., "Controlled Growth and Structures of Molecular-Scale Silicon Nanowires", *Nano Lett.*, vol. 4, pp. 433-436, March 2004.

[16] V. Schmidt, S. Senz, and U. Gosele, "Diameter-Dependent Growth Direction of Epitaxial Silicon Nanowires", *Nano Lett.*, Vol. 5**,** pp. 931-935, April 2005.

[17] M. Morales, and C.M. Lieber, "A Laser Ablation Method for the Synthesis of Crystalline Semiconductor Nanowires", *Science*, vol. 279, pp. 208-211, Jan. 1998.

[18] V. Schmidt, J.V. Wittemann, and U. Gösele, "Growth, Thermodynamics, and Electrical Properties of Silicon Nanowires", *Chem. Rev.*, vol. 110, pp. 361-388, Jan. 2010.

[19] A.K. Singh, V. Kumar, R. Note, and Y. Kawazoe, "Pristine Semiconducting [110] Silicon Nanowires", *Nano Lett.*, vol. 5, pp. 2302-2305, Oct. 2005.

[20] R. Kagimura, R.W. Nunes, and H. Chacham, "Structures of Si and Ge Nanowires in the Subnanometer Range", *Phys. Rev. Lett.*, vol. 95, pp. 115502 1-4, Sept. 2005.

[21] J.D. Prades, J. Arbiol, A. Cirera, and J.R. Morante, "Concerning the 506 cm^{-1} band in the Raman spectrum of silicon nanowires", *Appl. Phys. Lett.*, vol. 91, pp. 123107 1-3, Sept. 2007.

[22] J. Arbiol, B. Kalache, P. Roca i Cabarrocas, J.R. Morante, A. Fontcuberta i Morral, "Influence of Cu as a catalyst on the properties of silicon nanowires synthesized by the vapour-solid-solid mechanism", *Nanotechnology*, vol. 18, pp. 305606 1-8, May 2007.

[23] A. Fontcuberta i Morral, J. Arbiol, J.D. Prades, A. Cirera, and J.R. Morante, "Synthesis of Silicon Nanowires with Wurtzite Crystalline Structure by Using Standard Chemical Vapor Deposition", *Adv. Mater.*, vol. 19, pp. 1347-1351, May 2007.

[24] A. K. Buin, A. Verma, A. Svizhenko and M.P. Anantram, "Significant Enhancement of Hole Mobility in [110] Silicon Nanowires Compared to Electrons and Bulk Silicon", *Nano Lett.*, vol. 8, pp. 760-765, Jan. 2008.

[25] J.F. Justo, R.D. Menezes, and L.V.C. Assali, "Stability and plasticity of silicon nanowires: The role of wire perimeter", *Phys. Rev. B*, vol. 75, pp. 045303 1-5, Jan. 2007.

[26] P.B. Sorokin, *et al.*, "Density functional study of <110>-oriented thin silicon nanowires", *Phys. Rev. B*, vol. 77, pp. 235417 1-5, June 2008.

[27] A. Svizhenko, P.W. Leu, and K. Cho, "Effect of growth orientation and surface roughness on electron transport in silicon nanowires", *Phys. Rev. B*, vol. 75, pp. 125417 1-7, March 2007.

[28] F. Hernández-Ramírez, *et al.*, "Fabrication of Nanodevices Based on Individual SnO_2 Nanowires and Their Electrical Characterization", in *Metal Oxide Nanostructures and Their Applications*, Ed. A. Umar, by Americal Scientific Publishers (ASP), 2009. Chapter 1.

[29] P.R. Bandaru, and P. Pichanusakorn, "An outline of the synthesis and properties of silicon nanowires", *Semicond. Sci. Technol,.*vol. 25, pp. 024003 1-16, Feb. 2010.

[30] N. Seoane, A. Martinez, A.R. Brown, and A. Asenov, "Study of surface roughness in extremely small Si nanowire MOSFETs using fully-3D NEGFs", Proceedings of the 2009 Spanish Conference on Electron Devices – Feb 11-13, 2009. Santiago de Compostela, Spain.

[31] W. Kohn, and L.J. Sham, "Self-Consistent Equations Including Exchange and Correlation Effects", *Phys. Rev.,* vol. 140, pp. A1133-A1138, Nov. 1965.

[32] P. Hohenberg, and W. Kohn, "Inhomogeneus Electron Gas", *Phys. Rev.,* vol. 136, pp. B864-B871, Nov. 1964.

[33] J.M. Soler, *et al.*, "The SIESTA method for ab initio order-N materials simulation", *J. Phys.: Condens. Matter*, vol. 14, pp. 2745-2779, Mar. 2002.

[34] P. Ordejón, E. Artacho, and J.M. Soler, "Self-consistent order-N density-functional calculations for very large systems", *Phys. Rev. B*, vol. 53, pp. R10441-R10444, Apr. 1996.

[35] J.P. Perdew, K. Burke, and M. Ernzerhof, "Generalized Gradient Approximation Made Simple", *Phys. Rev. Lett.,* vol. 77, pp. 3865-3868, Oct. 1996.

[36] J.P. Perdew, *et al.*, "Restoring the Density-Gradient Expansion for Exchange in Solids and Surfaces", *Phys. Rev. Lett.*, vol. 100, pp. 136406 1-4, Apr. 2008.

[37] N. Troullier, and J.L. Martins, "Efficient Pseudopotentials for plane-wave calculations. II. Operators for fast iterative diagonalization", *Phys. Rev. B.*, vol. 43, pp. 1993-2006, Jan. 1991.

[38] L. Kleinman, and D.M. Bylander, "Efficacious Form for Model Pseudopotentials", *Phys. Rev. Lett.*, vol. 48, pp. 1425-1428, May 1982.

[39] E. Artacho, *et al.*, *User's Guide. SIESTA 3.0-beta*. Fundación General Universidad Autónoma de Madrid, Sep. 2009.

[40] J. Moreno, and J.M. Soler, "Optimal meshes for integrals in real- and reciprocal-space unit cells", *Phys. Rev. B*, vol. 45, pp. 13891-13898, Jun. 1992.

[41] H. Monkhorst, and J. Pack, "Special points for Brillouin-zone integrations", *Phys. Rev. B*, vol. 13, pp. 5188-5192, Jun. 1976.

[42] D. Sánchez-Portal, P. Ordejón, E. Artacho, and J.M. Soler, "Density-functional method for very large systems with LCAO basis sets", *Int. J. Quantum Chem.,* vol. 65, pp. 453-461, Dec. 1997.

[43] R. van Leeuwen, *et al.*, "Introduction to the Keldysh Formalism", *Lect. Notes Phys.*, vol. 706, pp. 33-59, Jan. 2006.

[44] M. Brandbyge, J.-L. Mozos, P. Ordejón, J. Taylor, and K. Stokbro, "Density-functional method for nonequilibrium electron transport", *Phys. Rev. B*, vol. 65, p. 165401 1-17, Mar. 2002.

[45] D. K. Ferry, S. M. Goodnick, and J. Bird, *Transport in Nanostructures.* New York: Cambridge University Press, 2009, Ch. 3.

[46] W.M. Yim, and R.J. Paff, "Thermal expansion of AIN, sapphire, and silicon", *J. Appl. Phys.*, vol. 45, pp. 1456-1457, Mar. 1974.

[47] M. Topsakal, V.M.K. Bagei, and S. Ciraci, "Current-voltage (I-V) characteristic of armchair grapheme nanoribbons under uniaxial strain", *Phys. Rev. B*, vol. 81, pp. 205437 1-5, May 2010.

[48] O.B. Malcioglu, and S. Erkoç, "Functionality of C(4,4) Carbon Nanotube as Molecular Detector", *Journal of nanoscience and nanotechnology*, vol. 8, p. 469-478, Feb. 2008.

[49] J.A Torres, "Ab initio simulations of the mechanics and electrical transport of Pt nanowires", *Science and Technology of Advanced Materials*, vol. 8, pp. 186-190, Apr. 2007.